PROGRAM

PNEUMATIC AND HYDRAULIC CONVEYING SYSTEMS II

June 20-25, 1999
Davos, Switzerland

Conference Chair:
Dr. Avi Levy
Department of Mechanical Engineering
Ben-Gurion University of the Negev - Beer-Sheva, Israel

Conference Co-Chair:
Dr. Tom Taylor
Unilever Research - UK

United Engineering Foundation, Inc.
Three Park Avenue, 27th Floor
New York, NY 10016-5902
T: 1-212-591-7836 - F: 1-212-591-7441
E-mail: engfnd@aol.com **WWW:** http://www.engfnd.org

DISCRETE WAVELETS FREQUENCY ANALYSIS FOR SPIRAL FLOW PNEUMATIC CONVEYING

Masahiro TAKEI
Nihon University, Tokyo Japan

Hui LI
Kagoshima University, Kagoshima Japan

Mitsuaki OCHI
Nihon University, Tokyo Japan

Yoshifuru SAITO
Hosei University, Tokyo Japan

Kiyoshi HORII
Shirayuri College, Tokyo Japan

ABSTRACT
Time-frequency distributions of axial turbulence velocities of spiral pipe flow and typical turbulence flow have been clearly decomposed in a range from low frequency level to high frequency level by means of discrete wavelets transform. As a result, the lower frequency levels (under Level 4) of the spiral flow are extremely lower as compared with those of the typical turbulence flow. Moreover, the spiral flow is dominated by Level 3 to be stabilized from the autocorrelation. The originality of this paper lies in applying discrete wavelets transform and its autocorrelation analysis to analyzing the spiral flow stable motion in time-frequency dimension.

KEYWORDS Discrete wavelets transform, Spiral flow, Frequency analysis, Turbulence velocity, Fluctuation level, Autocorrelation

1. INTRODUNCTION
Spiral flow is a swirling flow with large free vortex region, high concentration to the axis and high stability [1]. From the high stability characteristics, the spiral flow is useful for industrial applications such as optical cord installation in a small diameter pipeline with bends[2] and high performance pneumatic transportation without particles touching pipe inner wall[3]. The solids in the two-phase spiral pipe flow acquire their position in a pipeline without large vibration. The motivation behind this work is to clarify the mechanism of the high stability in order to improve the spiral flow system. Time-frequency analysis is a suitable method to analyze the stability as a first step.

Recently, wavelets transform has been popular for time-frequency analysis instead of Fourier transform in mechanical engineering fields. The merits of the wavelets analysis is to be able to analyze the frequency not to erase the time information. Wavelets transform [4] is roughly classified with two types, which are continuous wavelets transform and discrete wavelets transform. The continuous wavelets transform has been generally used for time frequency analysis in vibration wave. For example, self-similarity of the inner structure of the jet [5], the breakdown of a large eddy and the successive branching of a large eddy structure in a plane jet [6], decomposition of Reynolds stress in a jet [7], and the multiple acoustic modes and the shear layer instability [8] were investigated.

However, most of the researchers on the time-frequency analysis carried out the continuous wavelets transform. On the other hand, the discrete wavelets transform has been mainly used for picture image processing. The analysis enables to decompose and to compose picture image data quantitatively because of the orthonormal transform. Saito applied this idea to analyzing the electromagnetic wave[9].

The originality of this paper lies in applying discrete wavelets transform and autocorrelation to each frequency level to analyzing the spiral flow stable motion. In this paper, as a first step to clarify the stability, time-frequency distribution of axial turbulence velocity of spiral pipe flow is decomposed from low frequency level to high frequency level by discrete wavelets transform and its autocorrelation. It is recognized which level is dominant to stabilize the spiral flow.

2. THEORY OF DISCRETE WAVELETS TRANSFORM
2.1 Basic Concept Using Simple Base Function
Basic concept of discrete wavelets transform is described using matrix expression instead of integral expression. One dimensional input data matrix with four elements **X** and an analyzing wavelets matrix of Haar base function **W** are used to simplify the expression. For example, the input data matrix **X** is discrete velocity data with time. The wavelets transform matrix S that indicates wavelets spectrum is expressed by

$$\begin{bmatrix} S_1 \\ D_1 \\ d_1 \\ d_2 \end{bmatrix} = \left(\frac{1}{\sqrt{2}}\right)^2 \begin{bmatrix} 1 & 1 & 1 & 1 \\ 1 & 1 & -1 & -1 \\ \sqrt{2} & -\sqrt{2} & 0 & 0 \\ 0 & 0 & \sqrt{2} & -\sqrt{2} \end{bmatrix} \begin{bmatrix} a \\ b \\ c \\ d \end{bmatrix} \quad \text{——(1)}$$

or $\mathbf{S} = \mathbf{W} \cdot \mathbf{X}$ ——(2)

Where, $\mathbf{W^T \cdot W = I}$, **I** is a unit matrix and $\mathbf{W^T}$ is a transpose matrix of **W**. The analyzing wavelets matrix is an orthonormal. In Eq. (1), the first element in the wavelets spectrum S_1 shows a transform to obtain a mean value with a weight on the all input data, $a+b+c+d$. The second element in the wavelets spectrum D_1 shows a transform to obtain a difference value between the fast half and the latter half with a weight on the input data, $\{(a+b)-(c+d)\}$. It means that this element includes the lower frequency level of the input data. The third element d_1 shows a transform to obtain a difference value on the first half of the input data, $(a-b)$. The fourth element d_2 is a transform to obtain a difference value on the latter half, $(c-d)$. The third and forth elements include the higher frequency level of the input data. Therefore, the input data is able to classified to a range from higher frequency level to lower frequency level. Because of orthonormal, the inverse discrete wavelets transform is expressed by,

$$\mathbf{X} = \mathbf{W^T \cdot S} \quad \text{——(3)}$$

Moreover, from Eq. (3), the input data **X** is decomposed by multiresolution. The matrix expression is

$$\begin{bmatrix} a \\ b \\ c \\ d \end{bmatrix} = \left(\frac{1}{\sqrt{2}}\right)^2 \begin{bmatrix} 1 & 1 & \sqrt{2} & 0 \\ 1 & 1 & -\sqrt{2} & 0 \\ 1 & -1 & 0 & \sqrt{2} \\ 1 & -1 & 0 & -\sqrt{2} \end{bmatrix} \begin{bmatrix} S_1 \\ D_1 \\ d_1 \\ d_2 \end{bmatrix} = \mathbf{W^T} \begin{bmatrix} S_1 \\ 0 \\ 0 \\ 0 \end{bmatrix} + \mathbf{W^T} \begin{bmatrix} 0 \\ D_1 \\ 0 \\ 0 \end{bmatrix} + \mathbf{W^T} \begin{bmatrix} 0 \\ 0 \\ d_1 \\ d_2 \end{bmatrix} \quad \text{——(4)}$$

or $\mathbf{X = W^T S = W^T S_0 + W^T S_1 + W^T S_2}$ ——(5)

Where, $\mathbf{S_0} = [S_1\ 0\ 0\ 0]^T$ $\mathbf{S_1} = [0\ D_1\ 0\ 0]^T$ $\mathbf{S_2} = [0\ 0\ d_1\ d_2]^T$. $\mathbf{W^T S_0}$, $\mathbf{W^T S_1}$ and $\mathbf{W^T S_2}$ are called Level 0, Level 1 and Level 2, respectively.

2.2 Generalization of Discrete Wavelets Transform

Many orthonormal wavelets analyzing function are found [4]. The basic concept of the discrete wavelets transform is generalized by using fourth Daubechies function (N=4). The analyzing wavelets matrix is also an orthonormal function. The analyzing wavelets matrix **W** is acquired by a cascade algorithm on the basis of a function matrix **C**. The matrix **C** is shown in Eq. (6),

$$\mathbf{C} = \begin{pmatrix} c_0 & c_1 & c_2 & c_3 & 0 & 0 & \cdots & 0 & 0 & 0 & 0 \\ c_3 & -c_2 & c_1 & -c_0 & 0 & 0 & \cdots & 0 & 0 & 0 & 0 \\ 0 & 0 & c_0 & c_1 & c_2 & c_3 & \cdots & 0 & 0 & 0 & 0 \\ 0 & 0 & c_3 & -c_2 & c_1 & -c_0 & \cdots & 0 & 0 & 0 & 0 \\ \cdot & \cdot & \cdot & \cdot & \cdot & \cdot & \cdots & \cdot & \cdot & \cdot & \cdot \\ 0 & 0 & 0 & 0 & 0 & 0 & \cdots & c_0 & c_1 & c_2 & c_3 \\ 0 & 0 & 0 & 0 & 0 & 0 & \cdots & c_3 & -c_2 & c_1 & -c_0 \\ c_2 & c_3 & 0 & 0 & 0 & 0 & \cdots & 0 & 0 & c_0 & c_1 \\ c_1 & -c_0 & 0 & 0 & 0 & 0 & \cdots & 0 & 0 & c_3 & -c_2 \end{pmatrix} \begin{matrix} c_0 = \frac{1+\sqrt{3}}{4\sqrt{2}} \\ c_1 = \frac{3+\sqrt{3}}{4\sqrt{2}} \\ c_2 = \frac{3-\sqrt{3}}{4\sqrt{2}} \\ c_3 = \frac{1-\sqrt{3}}{4\sqrt{2}} \end{matrix} \quad \text{——(6)}$$

$$c_3 - c_2 + c_1 - c_0 = 0 \text{——(7)} \qquad 0\,c_3 - 1\,c_2 + 2\,c_1 - 3\,c_0 = 0 \text{——(8)}$$

Where, $\mathbf{C^T \cdot C = I}$. The first line in Eq. (6) is called scaling coefficients and second line is called wavelets coefficients. Forth Daubechies function (N=4) has four coefficients in a line. The first line shows a transform to obtain a mean value with weights of c_0, c_1, c_2 and c_3 on the input data. The second line shows a transform to obtain a difference value with weights of c_0, c_1, c_2 and c_3 on the input data. The third line shows a transform to translate the first line by two steps. The fourth line is a transform to do the second line by two steps. Eqs. (7) and (8) show the transformed values are zero when the input data are constant or are simply increased. To explain easily the process to acquire the analyzing wavelets matrix **W** from **C**, the matrix **X** is assumed as one dimensional 16 elements,

$$\mathbf{X} = [x_1\ x_2\ x_3\ x_4\ x_5\ x_6\ x_7\ x_8\ x_9\ x_{10}\ x_{11}\ x_{12}\ x_{13}\ x_{14}\ x_{15}\ x_{16}]^T \quad \text{——(9)}$$

From Eqs. (6) and (9), the transformed matrix **X'** is

$$\mathbf{X'} = \mathbf{C_{16}X} = [s_1\ d_1\ s_2\ d_2\ s_3\ d_3\ s_4\ d_4\ s_5\ d_5\ s_6\ d_6\ s_7\ d_7\ s_8\ d_8]^T \quad \text{——(10)}$$

Where, $\mathbf{C_{16}}$ is 16X16 matrix of **C**. The element s indicates the mean value and the element d indicates the difference value. The elements in the matrix **X'** are replaced by a matrix $\mathbf{P_{16}}$.

$$\mathbf{P_{16}X' = P_{16}\,C_{16}X} = [s_1\ s_2\ s_3\ s_4\ s_5\ s_6\ s_7\ s_8\ d_1\ d_2\ d_3\ d_4\ d_5\ d_6\ d_7\ d_8]^T \text{——(11)}$$

Where, $\mathbf{P_{16}}$ is defined as

$$P_{16}=\begin{pmatrix}
1&0&0&0&0&0&0&0&0&0&0&0&0&0&0&0\\
0&0&1&0&0&0&0&0&0&0&0&0&0&0&0&0\\
0&0&0&0&1&0&0&0&0&0&0&0&0&0&0&0\\
0&0&0&0&0&0&1&0&0&0&0&0&0&0&0&0\\
0&0&0&0&0&0&0&0&1&0&0&0&0&0&0&0\\
0&0&0&0&0&0&0&0&0&0&1&0&0&0&0&0\\
0&0&0&0&0&0&0&0&0&0&0&0&1&0&0&0\\
0&0&0&0&0&0&0&0&0&0&0&0&0&0&1&0\\
0&1&0&0&0&0&0&0&0&0&0&0&0&0&0&0\\
0&0&0&1&0&0&0&0&0&0&0&0&0&0&0&0\\
0&0&0&0&0&1&0&0&0&0&0&0&0&0&0&0\\
0&0&0&0&0&0&0&1&0&0&0&0&0&0&0&0\\
0&0&0&0&0&0&0&0&0&1&0&0&0&0&0&0\\
0&0&0&0&0&0&0&0&0&0&0&1&0&0&0&0\\
0&0&0&0&0&0&0&0&0&0&0&0&0&1&0&0\\
0&0&0&0&0&0&0&0&0&0&0&0&0&0&0&1
\end{pmatrix} \quad \text{——(12)}$$

Moreover, from Eq. (11), the transform is continuously carried out by **C** and **P** without any operations to the difference values,

$$\mathbf{W^{(2)}X} = [S_1\ S_2\ S_3\ S_4\ D_1\ D_2\ D_3\ D_4\ d_1\ d_2\ d_3\ d_4\ d_5\ d_6\ d_7\ d_8]^T \quad \text{——(13)}$$

$$\mathbf{S} = \mathbf{W^{(3)}X} = [S_1\ S_2\ D_1\ D_2\ D_1\ D_2\ D_3\ D_4\ d_1\ d_2\ d_3\ d_4\ d_5\ d_6\ d_7\ d_8]^T \text{——(14)}$$

Where,

$$\mathbf{W^{(2)}} = (\mathbf{P_{16}'C'_{16}})(\mathbf{P_{16}C_{16}}) \quad \text{——(15)}$$

$$\mathbf{W^{(3)}} = (\mathbf{P_{16}''\ C_{16}''})(\mathbf{P_{16}'\ C_{16}'})(\mathbf{P_{16}C_{16}}) \quad \text{——(16)}$$

$$\mathbf{P_{16}'}=\begin{bmatrix}\mathbf{P_8}&\mathbf{0}\\ \mathbf{0}&\mathbf{I_8}\end{bmatrix}\mathbf{C_{16}'}=\begin{bmatrix}\mathbf{C_8}&\mathbf{0}\\ \mathbf{0}&\mathbf{I_8}\end{bmatrix}\mathbf{P_{16}''}=\begin{bmatrix}\mathbf{P_4}&\mathbf{0}\\ \mathbf{0}&\mathbf{I_{12}}\end{bmatrix}\mathbf{C_{16}''}=\begin{bmatrix}\mathbf{C_4}&\mathbf{0}\\ \mathbf{0}&\mathbf{I_{12}}\end{bmatrix} \quad \text{——(17)}$$

$\mathbf{W^{(3)}}$ is a analyzing wavelets matrix that is **W** in Eq. (2). The wavelets spectrum **S** in Eq. (2) is $\mathbf{W^{(3)}X}$ in Eq. (14). In Eq. (13), S_1 indicates the mean value from s_1 to s_4 in Eq. (11). S_2 indicates the mean value from s_3 to s_6 that translate by two steps. D_1 indicates the difference value from s_1 to s_4. In Eq. (14), S_1 indicates the mean value from S_1 to S_4 in Eq. (13). D_1 indicates the difference value from S_1 to S_4 in Eq. (13). From Eq. (14), the input data are transformed to the mean values and the difference values with valuable resolution levels by the discrete wavelets transform. The input data are divided into a range from high frequency to low frequency.

From Eq. (14), the inverse wavelets transform is,

$$\mathbf{X} = [\mathbf{W^{(3)}}]^T\mathbf{S} \quad \text{——(18)}$$

$$[\mathbf{W^{(3)}}]^T=[(\mathbf{P_{16}''C_{16}''})(\mathbf{P_{16}'C_{16}'})(\mathbf{P_{16}C_{16}})]^T = \mathbf{C_{16}}^T\mathbf{P_{16}}^T(\mathbf{C_{16}'})^T(\mathbf{P_{16}'})^T(\mathbf{C_{16}''})^T(\mathbf{P_{16}''})^T \quad \text{——(19)}$$

From Eq. (18), the multiresolution is,

$$\mathbf{X} = [\mathbf{W^{(3)}}]^T\mathbf{S} = [\mathbf{W^{(3)}}]^T\mathbf{S_0} + [\mathbf{W^{(3)}}]^T\mathbf{S_1} + [\mathbf{W^{(3)}}]^T\mathbf{S_2} + [\mathbf{W^{(3)}}]^T\mathbf{S_3} \quad \text{——(20)}$$

Where, $\mathbf{S_0} = [S_1\ S_2\ 0\ 0\ 0\ 0\ 0\ 0\ 0\ 0\ 0\ 0\ 0\ 0\ 0\ 0]^T$ $\mathbf{S_1} = [0\ 0\ D_1\ D_2\ 0\ 0\ 0\ 0\ 0\ 0\ 0\ 0\ 0\ 0\ 0\ 0]^T$

$\mathbf{S_2} = [0\ 0\ 0\ 0\ D_1\ D_2\ D_3\ D_4\ 0\ 0\ 0\ 0\ 0\ 0\ 0\ 0]^T$ $\mathbf{S_3} = [0\ 0\ 0\ 0\ 0\ 0\ 0\ 0\ d_1\ d_2\ d_3\ d_4\ d_5\ d_6\ d_7\ d_8]^T$ ——(21)

In the case of sixteen input data and fourth Doubechies, multiresolution indicates from Level 0 to Level 3. In general, in the case that input data is 2^n and Doubechies function is kth (N=k), the algorithm to obtain levels is shown in Fig. 1. The final wavelets spectrum is obtained after the wavelet transform in Eq (14) continues until the number of final summation elements is less than k.

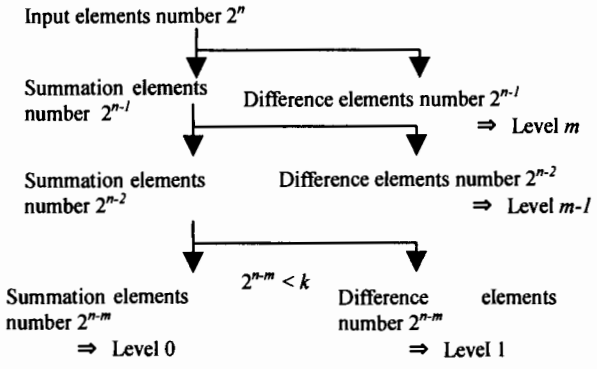

Fig. 1 Algorithm of discrete wavelets transform

3. EXPERIMENTS

3.1 Nozzle to Produce Spiral Flow

A nozzle to produce the spiral flow is designed with an annular slit connecting to a conical cylinder as shown in Fig. 2 [10]. Pressurized air is forced through the sides of the device into the buffer area, and then through the annular slit into a vertical pipe entrance. The suction force is generated at the back of the nozzle by Coanda effect. The annular flow, passing through the conical cylinder, develops a spiral structure with a steeper axial velocity and an azimuthal velocity distributions, even if it is not applied tangentially. Vaporized water as a tracer of LDV are sucked into the nozzle from the back of the nozzle. An ejector is used to generate the typical turbulence flow.

3.2 Experimental Equipment, Method & Conditions

The experimental equipment consisted of a vertical acrylic pipe, the nozzle to produce the spiral flow and an air compressor as shown in Fig. 3. The inside diameter of the vertical pipe was 41.0 mm. A LDV prove is set up at the side of the vertical pipe at 1.0 m from the air supply part to measure the axial velocity at the center of the pipe. He-Ne Laser power of LDV was 10 mW, and the probe picked up the reflected wave from the tracer. The air flow rate was 1.98 X 10^{-3} m^3/s. The mean velocity of the air flow in the vertical pipe calculated from the flow rate was 1.50 m/s. Reynolds number calculated from the mean velocity was about 4,200 .

The reflected wave pass though a timer unit connecting to LDV probe with 1ms (1,000 Hz) pick-up interval. The signals of the reflected wave were countered for about 5 seconds in a counter system connecting to the timer unit. The discrete sampling velocity data were n=1024(=2^{10}). The counter system has high pass and low pass filters that reduce signals under 0.625 m/s and over 6.25 m/s as noise. The pick up point is one point where is the center of the pipe as a first step study. The time mean velocities and turbulence levels of the spiral flow and typical turbulence flow are compared.

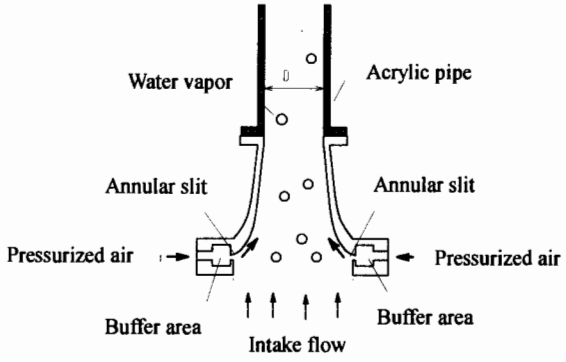

Fig. 3 Experimental equipment

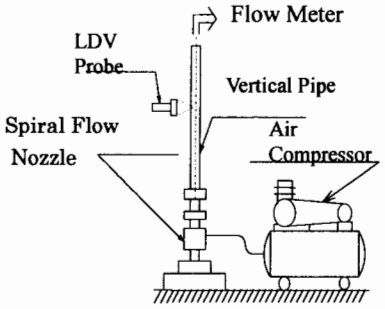

Fig.2 Spiral flow nozzle

3.3 Experimental Results

The velocities of the spiral flow and typical turbulence flow at the center of the pipe are obtained with LDV. The turbulence level is defined as,

$$v' = \frac{1}{n}\sum_{k=1}^{n}\left[\sqrt{(v_k - v_{mean})^2}\,/\,v_{mean}\right] \quad \text{——(22)}$$

Where, n is the sampling velocity number, v_{mean} is the time mean velocity, k is a pick-up time and v_k is kth pick-up velocity in a pick up time. The time-mean velocity and the turbulence level are shown in Table 1. From this table, the time mean velocity of the spiral flow is higher than that of typical turbulence flow by about 9 % even though the air flow rate is the same [1]. That is because the axial velocity of the spiral flow is steeper than that of the typical turbulence flow. Also, the turbulence level of the spiral flow is much lower than the typical turbulence flow by about 10 %. It means the spiral flow is a stable flow in an axial direction.

The normalized axial turbulence velocities in kth pick-up time with each mean velocity $v_k' = (v_k - v_{mean}) / v_{mean}$ are shown in Figs. 4 and 5. These figures are analyzed in the next section.

Table1 Time-mean velocity and turbulence Level

	Time mean velocity v_{mean}	Turbulence level v'
Spiral Flow	1.93 m/s	0.06616
Typical Turbulence Flow	1.77 m/s	0.07336

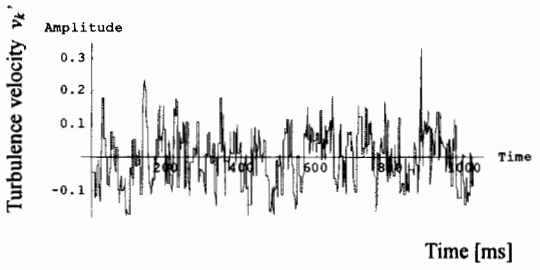

Fig. 4 Axial turbulence velocity of spiral flow

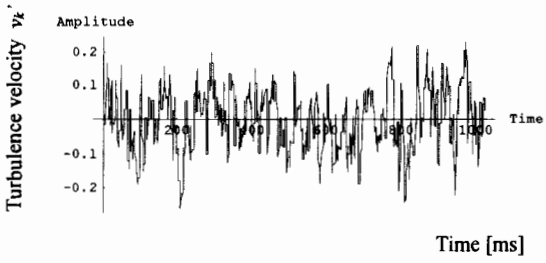

Fig. 5 Axial turbulence velocity of typical turbulence flow

4. ANALYSIS AND DISCUSSION

4.1 Analysis Method

The normalized axial turbulence velocities in Figs. 4 and 5 are analyzed by discrete wavelets transform and its autocorrelation. This wavelet analysis consists of three steps. Firstly, the 1024 ($=2^{10}$) sampling data of the axial turbulence velocities are put into the matrix **X** in Eq. (9). The matrix **X** is transformed to the wavelets spectrum **S** in the algorithm from Eq. (10) to Eq. (14). Next, the multiresolution analysis is carried out, that is, each part of the spectrum is inversely transformed to multiresolution levels by means of the discrete inverse wavelets transform in Eq. (20). Finally, autocorrelation of each level is obtained to recognize which level is dominant for the spiral flow stability.

Twentieth Daubechies function is used as an analyzing wavelets function. Twentieth Daubechies function has twenty coefficients from c_0 to c_{20} in the first line in Eq. (6), twenty coefficients from c_{20} to $-c_0$ in the second line in Eq. (6). In the case of twentieth Daubechies function and 1024 ($=2^{10}$) input data, the multiresolution classifies to seven levels as shown in Eq.(23).

$$\mathbf{X} = [\mathbf{W}^{(5)}]^{\mathrm{T}}\mathbf{S} = [\mathbf{W}^{(5)}]^{\mathrm{T}}\mathbf{S}_0 + [\mathbf{W}^{(5)}]^{\mathrm{T}}\mathbf{S}_1 + [\mathbf{W}^{(5)}]^{\mathrm{T}}\mathbf{S}_2 + [\mathbf{W}^{(5)}]^{\mathrm{T}}\mathbf{S}_3 + [\mathbf{W}^{(5)}]^{\mathrm{T}}\mathbf{S}_4 + [\mathbf{W}^{(5)}]^{\mathrm{T}}\mathbf{S}_5 + [\mathbf{W}^{(5)}]^{\mathrm{T}}\mathbf{S}_6 \quad \text{—(23)}$$

$\mathbf{W}^{(5)}$ indicates the five times operation to obtain Daubechies matrix from a matrix **C** in Eq. (6). The coefficients of twentieth Daubechies function are shown in Fig. 6. x axis shows the coefficients from c_{20} to c_0 in the second line of **C** matrix in Eq. (6). Therefore, 1 in x axis indicates c_{20}, 2 in x axis indicates c_{19}, and 20 indicates c_0 .

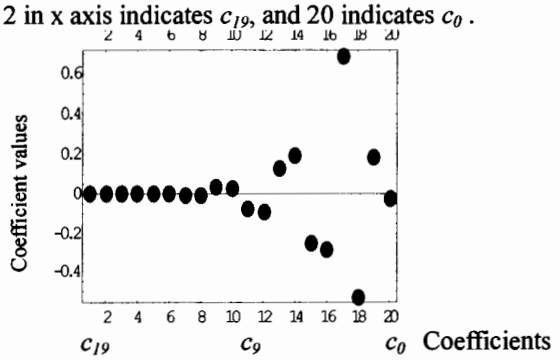

Fig. 6 Coefficients of twentieth Daubechies function

4.2 Turbulence Level on Each Frequency Level

To clarify the difference between wavelets transform and Fourier transform, the axial turbulence level on each frequency level defined in Eq. (24) is calculated before indicating the wavelets analysis.

$$V' = \frac{1}{n}\sum_{k=1}^{n}\left[\sqrt{(V'_k - V'_{levelmean})^2}\right] \quad \text{——(24)}$$

Where, the capital Vs indicate velocities on each wavelet level, in detail, $V'_{levelmean}$ is a time mean turbulence velocity and V'_k is a normalized turbulence velocity in kth pick-up time on each wavelet level. V' indicates a normalized turbulence level

in a wavelet level which includes a power spectrum obtained by Fourier transform. $V'_{levelmean}$ is not zero in the strict sense. The normalized turbulence level on each wavelet level V' is shown in Fig. 7 (Level 0 is not shown). From the other view, Fig.7 is a kind of power spectrum by Fourier Transform. From this figure, the turbulence levels of the spiral flow on all levels are lower than those of typical turbulence flow. Mainly, the level from Level 1 to Level 4 are remarkably different. Both turbulence levels have peaks at Level 3. The peak results from the energy contain range and the inertia range from Kolmogorov theory.

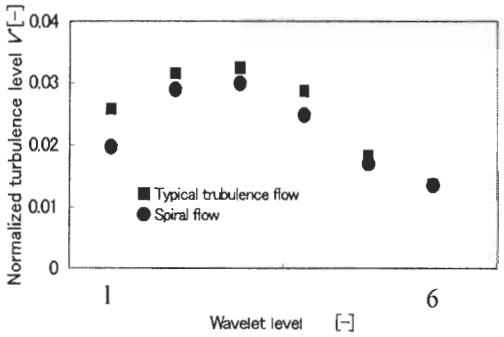

Fig. 7 Turbulence level on each frequency level

4.3 Wavelets Analysis Results & Discussion

Transforming inversely each level of the wavelets spectrum indicates multiresolution as shown in Eq.(20). Fig. 8(A) shows the multiresolution of the spiral flow, and Fig. 8(B) shows the multiresolution of the typical turbulence flow in three dimension display. They show the relation among the time, wavelet level and normalized turbulence velocity V_k'. From Fig. 8, it is recognized that time and frequency level is simultaneously analyzed. To clarify the each frequency level, Fig.8 is displaied in two dimension as shown in Fig. 9. From this multiresolution, the spectrum can be divided from low frequency level (Level 1) to high frequency level (Level 6). The summation from level 0 to level 6 recovers completely the original turbulence velocities in Figs. 4 and 5 (Level 0 is not shown). In the waveform on the low frequency level (Levels 1 and 2) in the figures, the turbulence velocity of the spiral flow is much smaller than this of the typical turbulence flow. The waveform on the middle frequency levels (Levels 3 and 4) is slightly different, and then, high frequency level is the same.

Next, the autocorrelation on each level in Fig. 9 is obtained to classify which level is dominant in the spiral flow with

$$R(\tau) = \frac{\overline{V'_k V'_{k+\tau}}}{\sqrt{\overline{V'^2_k}} \cdot \sqrt{\overline{V'^2_{k+\tau}}}} \qquad \text{——(25)}$$

τ is the delay time from 0.0 to 512 ms. The autocorrelation is done binarization with threshold value +0.25 and -0.25 because the periodisity makes clear. In this study, the points over +0.25 and under -0.25 of the autocorrelation is assumed to be high periodisity, and the points between -0.25 and +0.25 to be low periodisity. The binary autocorrelation is shown in Fig.10. In this figure, the black part is under -0.25, and white part is over +0.25, which are high correlation parts. The gray part is between -0.25 and +0.25, which is low correlation part. From this figure, it is recognized that Level 3 is dominant in the spiral flow because the black part and the white part are shown repeatedly.

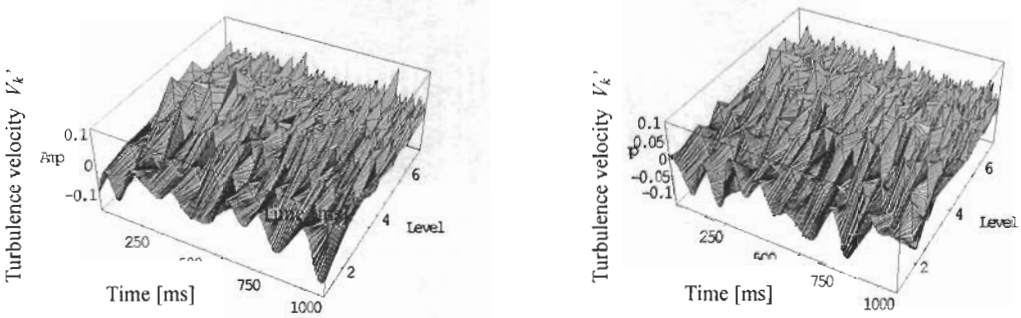

(A) Spiral flow **(B) Typical turbulence flow**

Fig. 8 Multiresolution analysis (3D Display)

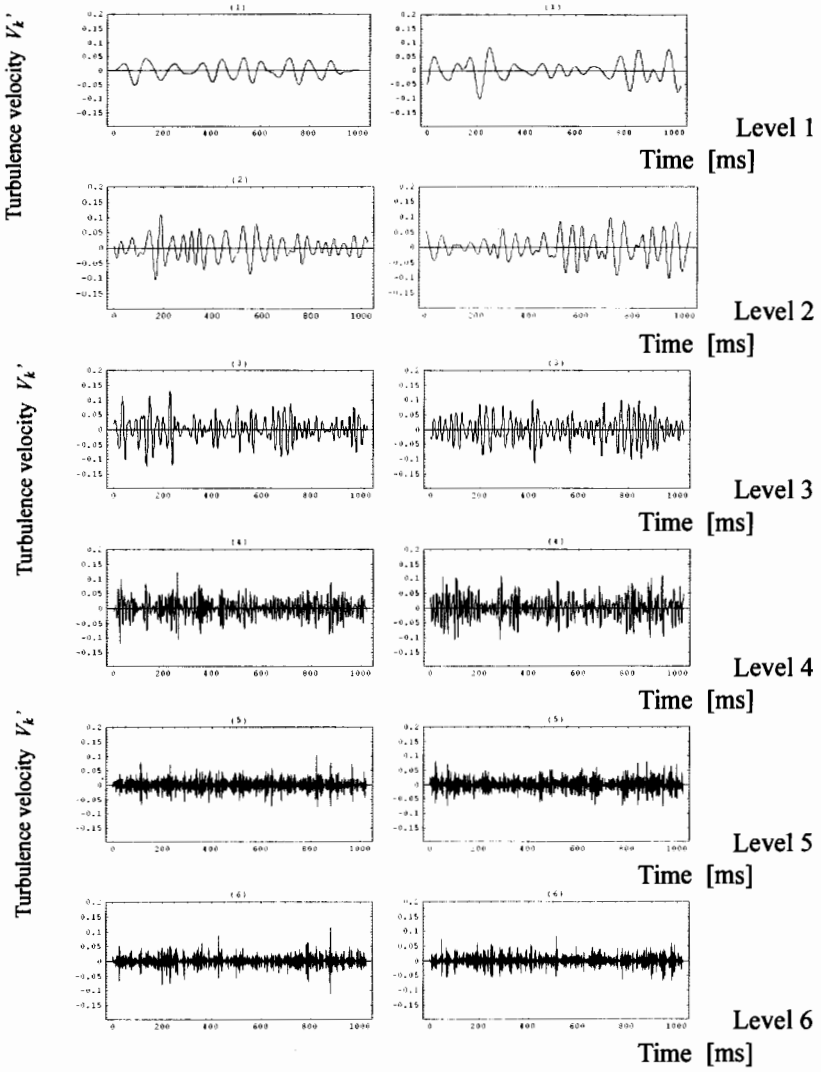

(A)Spiral flow (B) Typical turbulence flow

Fig. 9 Multiresolution analysis for turbulence velocity

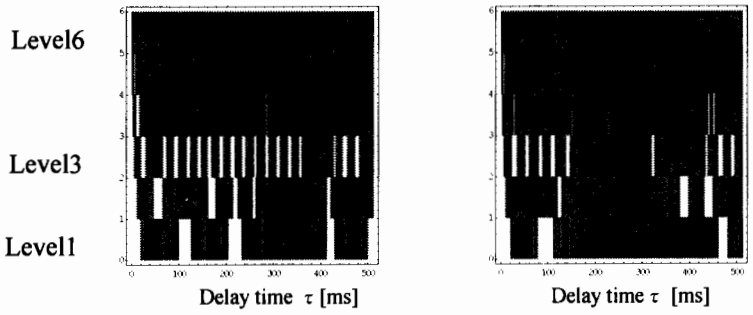

(A) Spiral flow (B) Typical turbulence flow

Fig. 10 Binary autocorrelation

5. CONCLUSIONS

Time-frequency distributions of axial turbulence velocities of spiral pipe flow and typical turbulence flow have been clearly decomposed in a range from low frequency level to high frequency level by means of discrete wavelets transform. Also, the dominant level to be stabilized is clasified. As a result, the following conclusions become clear.

(1) The time waveform on target level is able to extract by means of discrete wavelets transform and multiresolution because the orthonormal analyzing wavelets function composes and decomposes the original waveform. It is useful for analyzing the stability of spiral flow

(2) The axial turbulence level in the under middle frequency levels (under Level 4) of spiral flow are extremely lower as compared with that of typical turbulence flow.

(3) Level 3 of spiral flow has high periodisity. It means that the axial stability of spiral flow is mainly dominated by Level 3.

ACKNOWLEDGEMENTS

The authors are pleased to acknowledge the considerable assistance of Mr. T. Katayanagi and Mr. K. Kato in Nihon University.

REFERENCES

[1] Horii,K., (1990) Using Spiral Flow for Optical Cord Passing, *Mechanical Engineering - ASME*, Vol.112, No.8, pp68- 69

[2] Horii,K. et al.,(1991) A Coanda Spiral Device Passing Optical Cords with Mechanical Connectors Attached through a Pipeline, *ASME FED-Vol.121, Gas-Solid Flows,* pp65-70.

[3] Takei,M. et al., (1997) Transporting Particles without Touching Pipe Wall, *ASME FED,* FEDSM97-3629

[4] Molet,F. et al., (1989) Wavelet Propagation and Sampling Theory, *Geophysics*, Vol.11

[5]]Everson,R. and Sirovich,L., (1990) Wavelet Analysis to the Turbulence Jet, Phys.Lett., Vol.145 No.6, pp314-322

[6] Li,H. and Nozaki,T., (1995) Wavelet Analysis for the Plane Turbulence Jet (Analysis of large eddy structure), *JSME International Journal Fluids and Thermal Engineering*, Vol.38, No.4 pp525-531

[7] Gordeyev,S.V. and Thomas,F.O., (1995) Measurement of Reynolds Stress Reversal in a Planar Jet by Means of a Wavelet Decomposition, *Turbulent Flows ASME.* FED-Vol.208. pp.49-54

[8] Walker,S.H., Gordeyev,S.V. and Thomas,F.O., (1995)A Wavelet Transform Analysis Applied to Unsteady Jet Screech Resonance, *High speed jet flow ASME.* FED-Vol.214.pp103-108

[9] Saito,Y., (1996)Wavelet Analysis for Computational Electromagnetics, (in Japanese), *Trans. IEE of Japan,* Vol. 116A, No10, pp833-839

[10] Horii,K., (1988)*US.PAT. No.4,721,126, UK.PAT.* No.2, 180, 957